Article

Not peer-reviewed version

La-Modified SBA-15 Prepared by Direct Synthesis: Importance of Determining Actual Composition

Gloribel Morales-Hernández , José Escobar * , José Pacheco-Sosa , Mario A. Guzmán-Cruz , José G. Torres-Torres , Paz Del Angel-Vicente , María C. Barrera , Carlos E. Santolalla-Vargas , Hermicenda Pérez-Vidal

Posted Date: 21 May 2024

doi: 10.20944/preprints202405.1411.v1

Keywords: SBA-15; lanthanum; materials composition; platinum; phenol HDO

Article

La-Modified SBA-15 Prepared by Direct Synthesis: Importance of Determining Actual Composition

Gloribel Morales-Hernández [1], José Escobar [2,*], José G. Pacheco-Sosa [1], Mario A. Guzmán-Cruz [3], José G. Torres-Torres [1], Paz del Ángel Vicente [2], María C. Barrera [4], Carlos E. Santolalla-Vargas [5] and Hermicenda Pérez-Vidal [1]

[1] Universidad Juárez Autónoma de Tabasco, División Académica de Ciencias Básicas, Km. 1 Car. Cunduacán-Jalpa de Méndez, Col. La Esmeralda, 86690, Cunduacán, Tabasco, México
[2] Instituto Mexicano del Petróleo, Eje Central Lázaro Cárdenas Norte 152, San Bartolo Atepehuacan, G.A. Madero, Cd. de México, 07730
[3] Universidad Juárez Autónoma de Tabasco, División Académica Multidisciplinaria de Jalpa de Méndez, Carr. Estatal Libre Villahermosa-Comalcalco Km. 27+000 s/n Ranchería Ribera Alta, 86205, Jalpa de Méndez, Tabasco, México
[4] Facultad de Ciencias Químicas-Centro de Investigación en Recursos Energéticos y Sustentables, Universidad Veracruzana, Campus Coatzacoalcos, Av. Universidad km. 7.5, Col. Santa Isabel, Coatzacoalcos, Veracruz, 96538, México
[5] Departamento de Biociencias e Ingeniería, Centro Interdisciplinario de Investigaciones y Estudios sobre Medio Ambiente y Desarrollo (CIIEMAD), Instituto Politécnico Nacional, 30 de Junio de 1520 s/n, La Laguna Ticomán, G. A. Madero, 07340, Ciudad de México, México
* Correspondence: jeaguila@imp.mx

Abstract: La integration (at various nominal contents) in SBA-15 prepared under acidic medium was intended from corresponding direct nitrate addition during mesoporous silica formation. Materials were impregnated with Pt (1.5 w%) and studied through several textural (N_2 physisorption), structural (XRD, TG-DTG) and surface (FTIR, STEM-HAADF, SEM-EDS, NH_3 and CO_2 TPD) instrumental techniques. Pt-impregnated solids were tested in phenol hydrodeoxygenation (HDO, T=250 °C, 3.2 MPa, batch reactor, *n*-decane as solvent). Catalytic activity (in pseudo first order kinetic constant, k_{HDO} basis) was related to Pt dispersion which was, however, not determined by nominal rare earth content. Determining actual composition of modified SBA-15 materials is crucial in reaching sound conclusions regarding their physicochemical properties, especially when La modifier is directly added during mesoporous matrices formation where efficient interaction among constituents could be difficult to get. Otherwise, results from some characterization techniques (N_2 physisorption and FTIR, for instance) could be misleading and even contradictory. Indeed, extant modifier precursors when under SBA-15 synthesis conditions could affect the properties of prepared materials even though they were absent in obtained formulations. Performing a simple compositional analysis could eliminate uncertainties regarding the role of various modifiers on characteristics of final catalysts. However, several groups have failed in doing so.

Keywords: SBA-15; lanthanum; materials composition; platinum; phenol HDO

1. Introduction

SBA-15 materials possess interesting textural characteristics related to high surface area, tunable pore size and large pore volume. Also, thick walls (3-6 nm) could impart significant hydrothermal stability. Those Si-based mesostructured solids have been used as supports of various catalyst types due to their uniform porous network that could enhance reactants/products diffusion/counter diffusion to/from active sites. However, SBA-15 surface is not particularly suitable in dispersing phases to be impregnated mainly due to its inertness (very low acidity [1]). Significant efforts have

 doi:10.20944/preprints202405.1411.v1

been aimed on functionalizing those rather inert surfaces by introducing diverse inorganic/organic species that could be utilized to tailor silica surface to specific applications [2]. For instance, titania was efficiently introduced in SBA-15 matrices resulting in improved Pt dispersion [3]. However, method used to modify SBA-15 solids could be crucial determining textural, structural and surface properties of final doped materials. Regarding binary catalysts supports containing lanthanum our group reported on the properties in hydrodeoxygenation (HDO) reactions of Pt (1 wt%) supported on La-modified alumina where rare-earth at various contents was introduced by incipient wetness impregnation [4]. Beneficial effect on guaiacol HDO (as to material non modified by rare earth) conversion for catalyst was observed. However, selectivity to deoxygenated compounds decreased, those effects being related to surface basicity imparted by La domains. Thus, investigation on noble metal (NM) with La-SBA-15 supports was envisaged. Efficiently incorporating lanthanum to structured silica matrices could be difficult. For instance, it was reported [5] that instead of obtaining desired Si/La ratios (20 and 60, in SBA-15 solids) actual ones were much bigger where rare earth salt precursor was directly introduced during silica matrix synthesis. Authors claimed that those tiny quantities of incorporated La were due to high solubility of rare earth nitrate in the low pH reaction media. Thus, determining the actual amount of integrated modifier becomes crucial in relating the physicochemical properties of catalysts to their performance in various reactions. However, in several cases concentration of components was assumed, without analytically determining real ones. For instance, Roy et al [6] prepared V-modified SBA-15 (Si/V =20) from NH_4VO_3) directly added during SBA-15 hydrothermal synthesis under acidic medium (by HCL addition) used as support of Pt-Pd solids tested in toluene hydrogenation (HYD). The authors reported improved HYD over the V-modified material attributing that to enhanced noble metals (NM) dispersion. Although difficulty of heteroatoms integration in siliceous matrix prepared under acidic medium (due to V-O-Si linkages dissociation at low pH) was considered, prepared materials were characterized through some textural and surface techniques, but their composition was not actually determined. Thua, efficient vanadium integration in the SiO_2 was just assumed. Probably, that approach could be better applied in the case of catalysts obtained by post-synthesis modifier impregnation on already preformed SBA-15, where heteroatom deposition could be more controllable. As it could be seen from results reported in the present article, analysis through physicochemical characterization techniques could be misleading, if materials compositional analysis is not included.

In the present contribution, La integration (at various nominal contents) in SBA-15 matrices prepared through well-known protocol [7] was intended from corresponding nitrate addition during mesoporous silica formation (acidic medium). Materials were impregnated with Pt (1.5 w%) and studied through several textural, structural and surface instrumental techniques. Catalysts were tested in phenol (*P*, model species representing oxygenated aromatics in depolymerized lignin [8]) hydrodeoxygenation (HDO). Catalytic activity was related to NM dispersion which was, however, not determined by nominal rare earth content in the supports.

2. Results and Discussion

2.1. Materials Textural Properties

SBA-15 pristine matrix and corresponding La-modified materials had type IV N_2 adsorption isotherms (Figure 1 (a)) with H1 hysteresis, typical profiles of mesostructured solids with cylindrical pores [9]. No significant differences in shape were observed at increased nominal La concentration in reaction media, as opposed to the case of Ti-modified SBA-15 at various compositions [3], suggesting low rare earth-silica network interaction. However, important diminutions in N_2 adsorbed volume at saturation were registered for samples at various nominal rare earth contents. Changes in pore volume did not follow definite trend with lanthanum concentration, although those of doped solids were all minor to that of pristine SBA-15. Textural properties of studied carriers did not show (Table 1) correspondence with nominal amounts of lanthanum modifier used. As reference, theoretical surface area of binary solids considering incorporation of non-porous La_2O_3 component in SBA-15 matrices ($^bS_{BET}$) were included (fifth column, Table 1). Ratio of actual surface area respecting theoretical value for solids at given La_2O_3 content, did not show good concordance (excepting La8)

 doi:10.20944/preprints202405.1411.v1

for solids at several nominal La concentration. SBA-15 pore size distribution (PSD, from Barret-Joyner-Halenda method, BJH, desorption data branch) was alike to those previously reported (maxima at ~6 nm accompanied by minor peak at ~4 nm) when studying corresponding Ti-modified solids [3], Figure 1 (b). Although shift to lower diameter (just for major peak) was registered for La-modified samples, in general PSD was alike to that of pristine SBA-15. Again, that suggested weak La-SBA-15 interaction, if any. However, all in all, differences found mainly in materials surface area and pore volume pointed out to some structural modifications in mesoporous SiO_2 matrices by rare earth addition.

Table 1. Textural properties of SBA-15 and modified materials at several nominal La contents.

Sample	S_{BET} (m^2g^{-1})	V_P (cm^3g^{-1})	[a]D_P Peak 1	(nm) Peak 2	[b]S_{BET} (m^2g^{-1})	$S_{BET}/^bS_{BET}$
SBA-15	793	0.98	3.98	6.6	-	
La1	706	0.78	4.09	5.10	785	0.90
La2	582	0.61	3.93	5.66	777	0.75
La4	674	0.75	3.89	5.60	761	0.89
La8	685	0.76	3.86	5.58	730	0.94

[a]from BJH plot, desorption branch data. [b]Theoretical value considering well-dispersed non-porous La_2O_3 phase component.

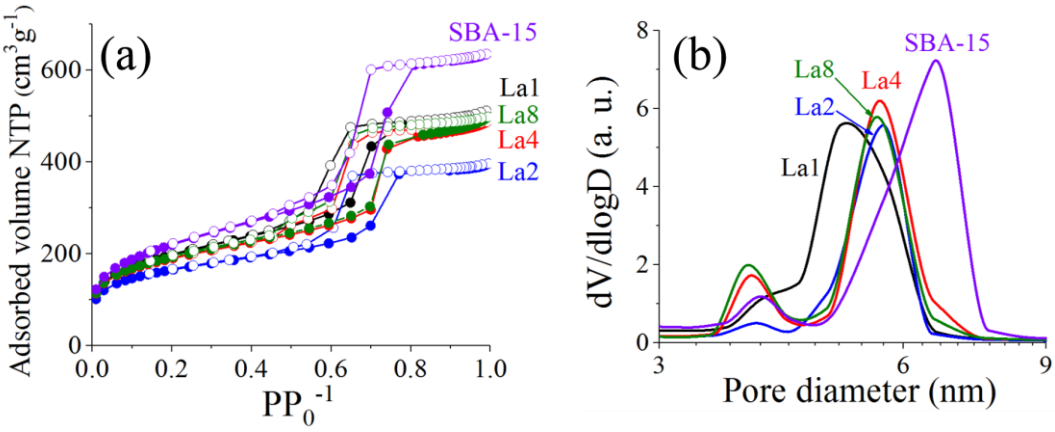

Figure 1. (a) N_2 adsorption isotherms (at -196 °C) of pristine SBA-15 and corresponding La-modified materials at various nominal contents. Open symbols: desorption branch; (b) Pore size distribution (BJH, desorption branch data) of studied solids. Formulations calcined at 500 °C.

After Pt loading, surface area and pore volume of studied materials suffered significant losses respecting those of corresponding supports, in spite of low NM loading (Figure S1 and Table S1). Conversely and with PLa2 as sole exception, corresponding PSD profiles remained essentially unaltered after Pt deposition, Figure S1 (b).Those data suggested NM particles at low dispersion being big enough to partially plug carriers porosity,

2.2. X-ray Diffraction

Wide signals in 15-35° 2θ range in diffractograms of studied samples corresponded to amorphous silica constituting SBA-15 walls [10], Figure 2. Peaks at 39.85, 46.3 and 67.6° (2θ values) of NM-containing formulations belonged to (111), (200) and (220): face-centered cubic metallic platinum facets. No PtO_x species were identified although studied solids were analyzed by XRD after calcining (500 °C, 6 h, under air), no reduction treatment being carried out. NM autoreduction of tetrammine platinum species after high-temperature calcination has been reported in the past [11]. Also, our group evidenced NM autoreduction when using H_2PtCl_6 as precursor salt deposited on SBA-15 modified matrices [3]. More studies on the effect of different Pt precursors on final catalysts properties are obviously needed [12]. Pt crystal size (from Scherrer formula, averaged from (111),

 doi:10.20944/preprints202405.1411.v1

(200) and (220) reflections, Table 2) augmented in PLa4 (see the most intense Pt (111) signal, Figure 2) as to the rest of samples. In any case, all impregnated solids had well defined peaks, pointing out sintering due to weak interaction with carriers. Determined crystal sizes (Table 2) were rather similar to those observed over catalysts supported on SBA-15 modified by various Ga contents and at similar NM loading [13]. Pt autoreduction could lead to crystals agglomeration in samples in weak interaction with the carrier [11]. Low NM dispersion could justify significant S_{BET} loss of supported samples much larger to those expected considering Pt loading (column 6, Table S1) due to crystals big enough to partially plug pores of used carriers.

Table 2. Pt crystal size of various NM-impregnated materials prepared, as determined by Scherrer formula using Pt (111), (200) and (220) reflections (peaks shown in Figure 2).

Catalyst	Crystal size (nm)
PSBA-15	22.3
PLa1	23.6
PLa2	27.9
PLa4	32.8
PLa8	21.2

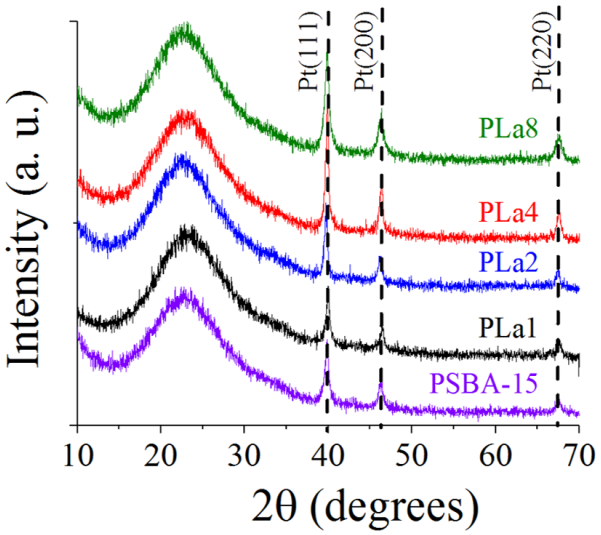

Figure 2. Wide-angle X-ray diffraction patterns of platinum (1.5 wt%) over SBA-15 and corresponding La-modified solids at various nominal contents.

2.3. FTIR Characterization

Infrared signals observed in all solids (Figure 3) corresponded to those well-known for SBA-15 materials [3]. Shifts to higher wavenumbers in absorption band at 958-960 cm^{-1} in SBA-15 (corresponding to Si-OH asymmetric stretching vibrations [14]) has been considered evidence of La intrusion in silica networks that hypsochromic displacement being function of rare earth concentration [15]. In our case, blue-shifted signals were observed for dopant-containing samples (Figure 3 and Table 3) suggesting La incorporation in SiO_2 network. However, those shifts have been also reported in Rh (1 wt%, deposited by incipient wetness impregnation) over SBA-15 due to the effect of NM impregnation on Si-O- vibration [16]. The signal observed at 2361 cm^{-1} (more notable in PSBA-15 spectrum) accompanied by small humps) at approximately 1633, 1441 and 1256 cm^{-1} could be related to physisorbed non-dissociated CO_2 [17]. Also, contributions from linearly adsorbed carbon dioxide could be related to absorptions at ~2320 cm^{-1} [18]. However, no defined carbonates-bicarbonates signals (1800-1200 cm^{-1} region) were clearly identified suggesting no significant amount

 doi:10.20944/preprints202405.1411.v1

of basic sites on analyzed materials. It is worth mentioning, that, expectedly, La addition could contribute on enhancing basic properties of corresponding rare earth containing surfaces [19].

Table 3. Hypsochromic shifts in the 955 cm^{-1} band of SBA-15 and NM-impregnated solids at several La nominal contents.

Sample	Peak position (cm^{-1}))
SBA-15	955
PSBA-15	959
PLa1	961
PLa2	964
PLa4	968
PLa8	971

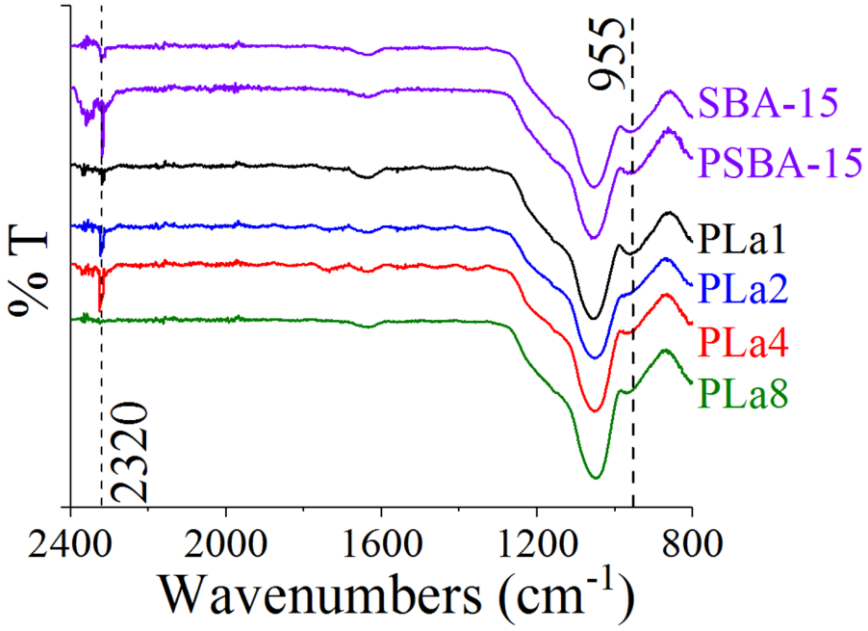

Figure 3. FTIR spectra of pristine SBA-15 and various La-modified supports at several nominal rare earth contents. (a) Carbonates (CO_2 adsorption) zone; (b) Blue-shift of Si-O-H asymmetric stretching vibration at ~955 cm^{-1}.

2.4. STEM (HAADF) Studies

In HAADF-STEM a finely focused probe of high energy electrons from STEM is scanned through a thin sample. Part of electronic beam could be scattered at larger angles to be collected by an annular detector then being used to create Z-contrast image. Considering that cross-section of this type of scattering depends upon squared atomic number (Z) of analyzed atoms (i.e., Z^2), corresponding micrographs enable chemical analysis due to image contrast where heavier atoms (NM ones) look brighter than those from silica carrier [20]. Thus, Pt crystals (around ~10 nm) were clearly identified on PLa4 (the sample containing the highest proportion of the smallest particles, as it will be further shown), Figure 4 (a). Meanwhile, honeycomb-like mesoporous structure (uniform channels along pores axes) [3] could be observed in background in mentioned micrograph. No segregated La domains were observed. Also, bigger sinterized particles were identified for that solid, Figure 4 (b). From particle size measurements corresponding histograms were obtained, Figure 5. According to them, PLa4 had enhanced amounts of smaller NM crystals. In the opposite, PSBA-15 and PLa1 showed larger proportion of bigger Pt particles (Figure 4 (c) and (d)). NM crystal size of various solids as determined from XRD (Table 2) could not coincide with those measured by electron microscopy

 doi:10.20944/preprints202405.1411.v1

as particles below 3-4 nm could not be detected by the former technique. Differently to beneficial influence of titanium content on Pt dispersion over SBA-15 [3], no positive influence of nominal La concentration in studied solids was evidenced, pointing out to weak (if any) interaction) between those species (see large NM particle in Figure 4 (b and (d)).

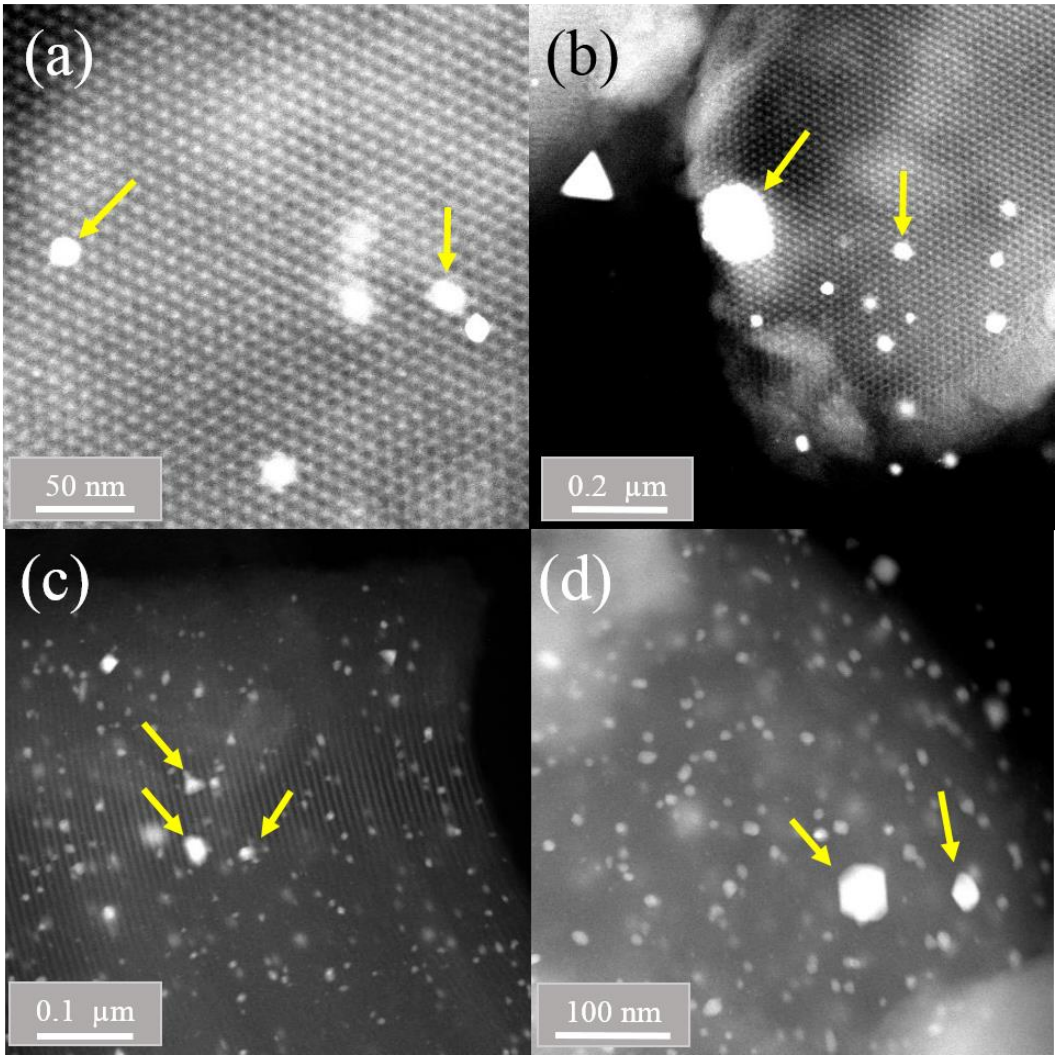

Figure 4. STEM (HAADF) micrographs of PLa4 ((a)-(b)) and PLa1 ((c)-(d)) solids Pt (1.5 wt%)/over supports prepared at different nominal rare earth content Unreduced calcined catalysts (500 °C). Arrows: NM crystals.

 doi:10.20944/preprints202405.1411.v1

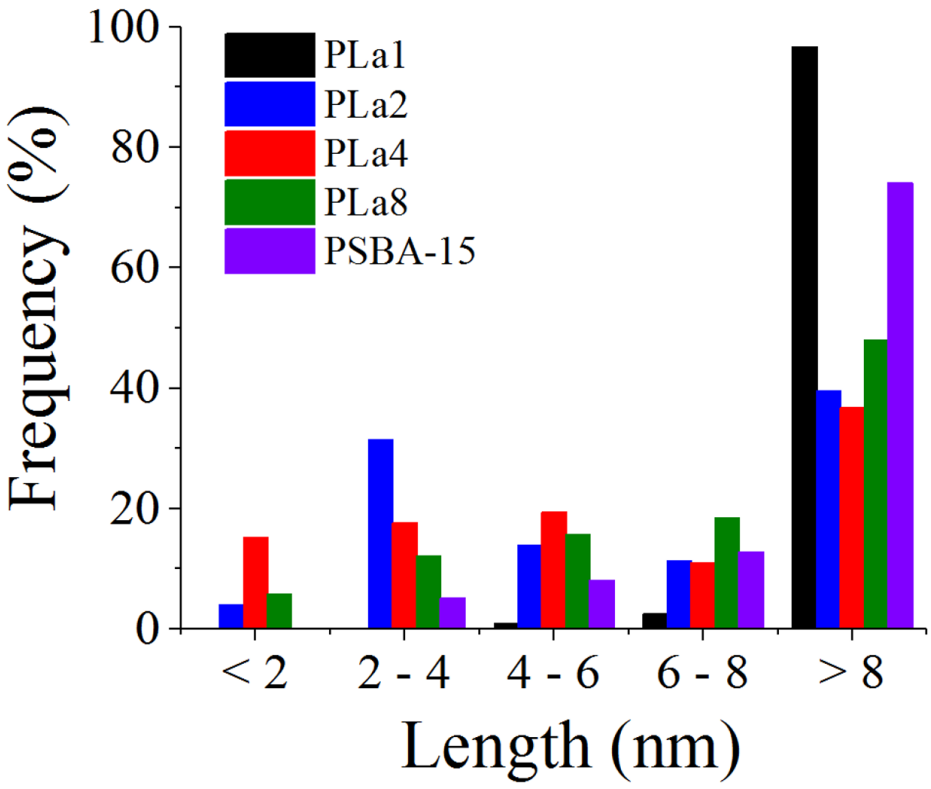

Figure 5. Histograms of Pt particle size over various prepared supports at different La nominal content (from STEM-HAADF).

2.5. HDO Reaction Test

Pt over various supports has been studied in HDO reactions of several feedstocks meanwhile SBA-15 has been used as corresponding carrier. [21]. Solids containing Pt over SBA-15 have been studied in *m*-cresol HDO [22] as well**.** Also, the **e**ffect of rather basic dopants (niobium in this case) on properties of SBA-15 Ni catalysts carrier was also studied in anisole HDO [23]. The effect of various metals (Nb, Ru, Pd, Pt) supported on SBA-16 was tested in phenol HDO [24] as well.

Prepared materials performance in *P* HDO was compared on k_{HDO} basis (Figure S2 and Table 4). The least active solids were PSBA-15 and PLa8, in strong agreement with their lower NM dispersion (Figure 5). In the opposite, PLa4 promoted the highest conversion, in accordance with its diminished particle size (Figure 5.). Thus, inverse correlation between metallic crystallites dimensions and *P* transformation capabilities was evidenced. Similar trend (specific activity per gram of Pt inversely proportional to Pt particle size) was observed in anisole HDO over Pt/SBA-15 [25]. Interestingly, production of deoxygenated compounds requires acid sites [25,26], Considering that *CH* was produced in our case and that silica surface lacks acidity [1] it could be possible that some oxidized PtO_x species (catalysts were not submitted to reduction) could provide the needed acid sites as proposed by others where it was considered that water produced under HDO conditions could partially oxidize metals generating acid centers [27]. That is a point that deserves further studies. No definitive trend on either *P* HDO activity or selectivity due to effect of nominal rare earth content was disclosed (Table 4). Thus, surface characterization of various NM-impreganted materials was devised to try to elucidate the reason of that unexpected behavior.

 doi:10.20944/preprints202405.1411.v1

Table 4. Pseudo first order kinetic constants (phenol HDO) over various supported NM catalysts prepared. T=250 °C, P=3.2 MPa, *n*-decane as solvent, batch reactor, ~107 rad s^{-1} (~1000 rpm) mixing speed.

Sample	k_{HDO} ($\times 10^{-5}$) (s^{-1})
PSBA-15	0.3
PLa1	2.0
PLa2	2.0
PLa4	3.0
PLa8	0.7

2.6. NH_3 and CO_2 Temperature-Programmed Desorption (TPD)

SBA-15 is well-known for essentially lacking either Lewis or protonic acidity [1]. Surprisingly, NH_3 TPD profiles for all studied materials were identical (Figure S3) displaying just a small amount of weak acid sites (Table S2). That was in full agreement with that reported for Pt/SBA-15 solids [28], where catalysts were tested in cellulose, hemicellulose and lignin catalytic pyrolysis. Very limited deoxygenation was observed over solids of low acidity, in concordance with that previously commented [4] Then, CO_2 TPD was carried out to analyze La contribution on basic sites creation [19,29]. Again, corresponding TPD profiles of studied samples were very similar one to another pointing out to no basic sites attributable to lanthanum nominal content (Figure S4, Table S3). CO_2 adsorption has been directly related to surface rare-earth coverage over La-alumina supports [30]. Thus, in our case, observed data suggested absence of surface La domains. The small hump around 90 °C has been related to very weakly adsorbed (physisorbed indeed) CO_2 [31,32]. Otherwise, SBA-15 modification with basic agents could be reflected in creation of surface sites able to retain CO_2 at high temperatures (by carbamates formation, for instance [32]).

2.7. Thermal Analysis

La8 (and corresponding Pt-impregnated solid, PLa8), the sample of highest nominal La content, and parent SBA-15 (as reference) calcined materials were studied by TG-DTG to determine carbonates (from atmospheric CO_2 adsorption on basic sites, if the case) presence. No additional signals as to that from mesoporous silica were observed (Figure S5) pointing out, again, rare earth absence on La8. Otherwise, carbonates decomposition could have been identified [4].

2.8. SEM-EDS Analysis

SBA-15 morphology and those of samples at various nominal La contents (not shown) were similar one to another and to those already reported [3] exhibiting rounded faceted particles of around 3-4 μm. Regarding compositional analysis, EDS has been considered very reliable technique, as compared to more complicated and expensive inductively coupled plasma (ICP) one [33]. Unexpectedly, no lanthanum was identified in any support sample (Table 5). These findings meant that La integration to silica network was not possible under acidic SBA-15 synthesis medium [5]. One important point to consider was that if actual materials composition has not been determined results from some characterization techniques (textural and IR studies, for instance) could have been misleading. Thus, wrong conclusions could have been reached by relating trends found in catalytic activity in *P* HDO to those data. It seems that textural properties changes due to nominal La content in various supports (Table 1) could have been provoked by presence of La salt during SBA-15 synthesis. Those domains, however, were evidently lixiviated under acidic media used [3,4]. It is worth nothing that those textural modifications could indeed affect NM dispersion (Figure 4 and 5), what could in turn influence HDO performance of various tested solids, without any direct influence of no extant rare earth domains. In the same direction, hypsochromic shifts on 955 cm^{-1} band of SBA-15 solids at several nominal La concentrations (Table 3) could originate misinterpretations, in absence of compositional data (Table 5). Indeed, other groups have reported NM phases on V-modified SBA-

 doi:10.20944/preprints202405.1411.v1

15 carriers but composition was not determined making difficult to assess the actual effect of vanadium integration during mesoporous silica synthesis. A similar situation was reported by Han et al. [15] when studying La-modified MCM- 41 as support of CO methanation Ni catalysts. In this case, again, no actual rare earth content in samples were determined, in solids where La salt was added during silica network preparation (under alkaline conditions). Our group has reported [29] on La incorporation at different contents (through corresponding nitrates) during sol-gel alumina synthesis those binary materials being used as hydrotreating catalysts (Co-Mo-P) supports. During active phases precursors impregnation through one-pot acidic (pH~1) solutions La was lixiviated provoking strong structural collapse reflected in significant textural loses. Conversely to that found in present communication, lixiviated La remained in catalysts formulations (determined by EDS) as one-pot deposition of Co-Mo-P was carried out by incipient wetness followed by drying and calcining. That was also proven by carbonates formation during corresponding CO_2 adsorption IR analyses [29].

Table 5. EDS analyses of prepared supports at various nominal rare earth contents.

Sample	O	Si	La
SBA-15	52.94	47.06	0.00
La1	49.49	50.50	0.02
La2	49.15	50.85	0.00
La4	46.63	53.27	0.10
La8	47.52	52.39	0.10

Summarizing, determining actual composition of modified SBA-15 materials is crucial to reach sound conclusions regarding their physicochemical properties. Although it could be reasonable considering well-integrated components when added by impregnation or deposition techniques are used [5], getting efficient interaction among constituents could be more difficult when corresponding modifications is tried during pristine matrices direct synthesis (under acidic medium)

Last but not least, research on the actual effect of La at various contents (loaded by pore-filling impregnation) on catalytic properties of Pt/SBA-15 solids in phenol HDO is in due course and will be the subject of upcoming reports.

3. Experimental

3.1. Material Synthesis

3.1.1. La-Modified SBA-15

To prepare SBA-15 protocol based on that proposed in [7] was carried out. Reactants and their amounts used were as described in [3]. Corresponding rare earth modified materials (at 1, 2, 4 and 8 wt% La_2O_3, La*c*, *c* lanthanum oxide nominal content) were synthesized similarly as Ti-containing ones described in [3], just utilizing required amounts of $La(NO_3)_3 \bullet 6H_2O$ (Sigma-Aldrich, 99.999%) instead of titanium precursor.

3.1.2. Pt-containing La-modified SBA-15

Regarding Pt-impregnated (1.5 wt%) carriers they were obtained by incipient wetness using tetraammine platinum (II) nitrate ($Pt(NH_3)_4(NO_3)_2$, Aldrich, 99,9 %). The rest of preparation steps of NM-containing solids were entirely similar to those used during Pt loaded materials synthesized in [3]. Totality Pt impregnation on supports was assumed (due to pore-filling technique used). Then, platinum loading refers to nominal value. Key PLa*c* was used to identify NM-loaded materials at various rare earth nominal concentrations.

 doi:10.20944/preprints202405.1411.v1

3.2. Materials Characterization

Texture (surface area, pore size distribution (PSD) and pore volume) and structural order of various studied solids were studied by N_2 physisorption and X-ray diffraction, respectively. Further details can be found elsewhere [3]). Pt crystal size of various NM-impregnated materials prepared were determined by Scherrer formula using Pt (111), (200) and (220) reflections using XPert HighScore Plus software. Fourier transform infrared spectra (FTIR) of prepared materials were obtained through Fourier transform infrared spectroscopy using Perkin Elmer Frontier equipment. Surface acidity and basicity of various materials were determined by temperature-programmed desorption (TPD) of NH_3 and CO_2, respectively, by using BELCAT-B (BEL Japan Inc.) equipment with thermal conductivity (TCD) detector. Typically, 500 mg samples were degassed under He (550 °C, 1 h). Then, for total acidity measurements solids were contacted with NH_3 (7% NH_3 balance He), 50 ml min^{-1} flow (30 min.). Then, the system was cooled-down to 40 °C under mixture flow (20 ml min^{-1}, 1 h). Weakly adsorbed NH_3 was eliminated through He flush (20 mL min^{-1}, 1 h). Finally, the temperature was increased to 550 °C (10 °C min^{-1}) to determine TPD profile. Regarding surface basicity studies, solids were firstly degassed under He flow (50 mL min^{-1}, 300 °C, 1 h). Then, samples were cooled-down to 50 °C under He flow (50 mL min^{-1}, 30 min). CO_2 adsorption was carried out (20 mL min^{-1}, 1 h). He flow was applied (20 mL min^{-1}, 50 °C, 30 min) to desorb weakly. retained (physisorbed) CO_2. Finally, CO_2 TPD profile was recorded in the 50-550 °C range (10 °C min^{-1}, heating ramp). Thermal profiles (TG-DTG) of some calcined materials were obtained by thermogravimetrical (TG) analysis. 15-50 mg samples were analyzed through TA instruments Q2000 equipment in the room temperature-550 °C range (heating ramp of 10 °C min^{-1}) under static air atmosphere. Differential thermogravimetric (DTG) profiles were obtained through derivative of corresponding TG curves. Particles morphology was studied through scanning electron microscopy (SEM), JEOL JSM-6010LA operating at 20 kV accelerating voltage, high vacuum and at various magnifications. Compositional analyses were carried out by attached EDS (Energy-Dispersive X-ray Spectroscopy) apparatus. Obtained micrographs were processed by InTouchScopeTM software. Materials were characterized by high-resolution transmission electron microscopy (HR-TEM) in Titan 80-300 microscope with a Schottky-type field emission gun operating at 300 kV. The point resolution and the information limit were better than 0.085 nm. HR-TEM digital images were obtained through CCD camera and analyzed by Digital Micrograph (GATANTM) software). Powdered materials were ultrasonically dispersed (ethanol) and supported on lacey carbon coated copper grids. Prepared solids were also studied by scanning transmission electron microscopy (STEM), micrographs being obtained in a JEOL JEM-2200FS with Schottky type field emission gun operating at 200 kV. High-angle annular dark field (HAADF) detector was used to acquire the images. To prepare the materials for observation, the powder samples were dispersed in ethanol and supported on Lacey Formvar-carbon coated Cu grid.

3.3. Phenol HDO Reaction Test

P HDO tests for various catalysts were carried out in batch system (Parr 4842), stainless steel, 100 ml vessel) operating at 250 °C, 3.2 MPa (initial H_2 pressure), 4 h. To discard external diffusion control vigorous stirring was used (>1000 rpm). Reaction mixture was composed by 0.2 g of catalyst to be tested, 0.3 g *P* in 100 ml *n*-decane (Sigma-Aldrich, ≥95%), *P* molar conc. [0.021], 460 ppm O. Tested catalysts were ground and sieved (U.S. mesh 80-100, ~165 μm particle size) to discard reaction control by internal diffusion phenomena [1]. NM-loaded solids were not submitted to reduction to avoid excessive active phase sintering as metallic Pt was identified in calcined samples (see section *2.2, XRD diffraction*). Liquid samples taken periodically were analyzed through gas chromatography (GC) in Varian Star 3400CX apparatus equipped with flame ionization detector, DB-5 non-polar capillary column ((5%-phenyl)-methylpolysiloxane), 30 m, 0.53 mm, 1.50 μm film thickness). At HDO conditions, *P* could be initially transformed by two main reaction pathways, HYD and direct deoxygenation (DDO), Scheme S1 [8]. The first one comprises aromatic ring saturation to cyclohexanone (HYD1 in Scheme S1) than could be transformed by subsequent saturation (HYD2 in Scheme S1) to cyclohexanol which dehydration leads to cyclohexane (*CH*, through cyclohexene

 doi:10.20944/preprints202405.1411.v1

intermediate) as final product. On the other hand, DDO takes place from C_{sp2}-O bond breaking conducting to benzene (*B*), followed by ring saturation (HYD4 in Scheme S1) to *CH*. In our case and according to retention times, the only peak detected was assigned to *CH*. As the non-polar GC column used separated species by boiling point (bp), some amounts of *B* in detected peak (attributed to *CH*) could not be ruled out due to those species very similar bp to each other. *P* conversion was calculated through determination of areas of corresponding chromatographic peak. Properties of various tested materials were compared on kinetic constant (k_{HDO}) basis considering pseudo first-order reactions (regarding *P* concentration, H_2 excess considered constant),

$$k_{HDO} = -\ln(1-x)/t \quad \textbf{(1)}$$

where:
x=*P* conversion at time *t*
t=reaction time (s)

4. Conclusions

Regarding SBA-15 modified by La addition, determining the actual materials composition is crucial, especially if the rare earth dopant is directly added during mesoporous silica network formation (under low pH conditions). Otherwise, results from some characterization techniques (N_2 physisorption and FTIR, for instance) could be misleading and even contradictory. Indeed, extant modifier precursors when under SBA-15 synthesis conditions could affect the properties of prepared materials even though they were absent in obtained | formulations. A simple compositional analysis could eliminate uncertainties regarding the role of various modifiers on characteristics of final catalysts.

Acknowledgments. The authors appreciate the generous financial support from MDPI for the publication of this manuscript. G. Hernández-Morales acknowledges financial support from CONAHCyT (México, Ph D grant 863718).

Supplementary Materials: The following supporting information can be downloaded at the website of this paper posted on Preprints.org. Figures: Impregnated solids characterization (N_2 physisorption); phenol HDO reaction scheme&kinetic constant calculation; NH_3&CO_2 TPD, TG-DTG analysis. Tables: Impregnated materials texture; NH_3&CO_2 TPD data.

Authors contributions: J. Escobar: conceptualization, methodology, investigation, data curation, manuscript writing. G.M.-H.: methodology, investigation, experimental. J.G.P.-S.: Experimental. M.A.G.-C.: Experimental. J.G.T.-T.: Experimental. P.A.V.: STEM-HAADF. M.C.B.: IR, TG, data curation, manuscript, tables, and plots editing. C.E.S.V.: phenol HDO. H.P.V.: administration.

Funding: This research was funded by UJAT-DACB.

Data availability statement: The data that support the findings of this study could be available under specific request.

Conflicts of interest: The authors declare no conflicts of interest.

References

1. Escobar, J.; Colín-Luna, J.A.; Barrera, M.C. Thioresistant PdPt/Al/SBA-15 for naphthalene hydrogenation. Ind. Eng. Chem. Res. 2024, 63(3), 1248-1260. DOI: 10.1021/acs.iecr.3c02359.
2. Zhang, P.; Wu, H.; Fan, M.; Sun, W.; Jiang, P.; Dong, Y. Direct and postsynthesis of Ti-incorporated SBA-15 functionalized with sulfonic acid for efficient biodiesel production. Fuel 2019, 235, 426-432. DOI:10.1016/j.fuel.2018.08.029.
3. Morales Hernández, G.; Pacheco Sosa, J. G.; Escobar Aguilar, J.; Torres Torres, J.G.; Pérez Vidal, H.; Lunagómez Rocha, M.A.; De la Cruz Romero, D.; del Ángel Vicente, P. Improving platinum dispersion on SBA-15 by titania addition. Rev. Mex. Ing. Chem. 2020, 19(2), 997-1010. DOI: 10.24275/rmiq/Mat821.
4. Escobar, J.; Barrera, M.C.; Santes, V.F.; Fouconnier, B. Guaiacol HDO on La-modified Pt/Al_2O_3: Influence of rare-earth loading. Can. J. Chem. Eng. 2023, 101(10), 5772-5784. DOI: 10.1002/cjce.24830.

 doi:10.20944/preprints202405.1411.v1

5. Bendahou, K.; Cherif, L.; Siffert, S.; Tidahy, H.L.; Benaïssa, H.; Aboukaïs, A. The effect of the use of lanthanum-doped mesoporous SBA-15 on the performance of Pt/SBA-15 and Pd/SBA-15 catalysts for total oxidation of toluene. Appl, Catal. A-Gen. 2008, 351, 82-87. DOI:10.1016/j.apcata.2008.09.001.
6. Roy, S.; Newalkar, B.L.; Datta, S. Vanadium Substituted SBA-15 Supported Bimetallic Pt, Pd Catalysts for Hydrogenation of Toluene to Methylcyclohexane. Can. J. Chem. Eng. 2014, 92, 1034-1040. DOI 10.1002/cjce.21978.
7. Flodström, K.; Alfredsson, V. Influence of the block length of triblock copolymers on the formation of mesoporous silica. Microporous and Mesoporous Mater. 2003, 59, 167-176. DOI: 10.1016/S1387-1811(03)00308-1.
8. Pinzón-Ramos, I.; Castillo-Araiza, C.O.; Tavizón-Pozos, J.A.; de los Reyes, J.A. On a Response Surface Analysis: Hydrodeoxygenation of Phenol over a CoMoS-Based Active Phase. Catalysts 2022, 12(10), 1139. DOI: 10.3390/catal12101139.
9. Leofanti, S.G.; Padovan, M.; Tozzola, G.; Venturelli, B. Surface area and pore texture of catalysts. Catal. Today (1998) 41, 207-210. DOI: 10.1016/S0920-5861(98)00050-9.
10. Palcheva, R.; Kaluža, L.; Dimitrov, L.; Tyuliev, G.; Avdeev, G.; Jirátová, K.; Spojakina, A. NiMo catalysts supported on the Nb modified mesoporous SBA-15 and HMS: effect of thioglycolic acid addition on HDS. Appl. Catal. A-Gen, 520, 24-34. DOI: 10.1016/j.apcata.2016.04.008.
11. Miller, J.T.; Schreier, M.; Kropf, A.J.; Regalbuto, J. R. A fundamental study of platinum tetraammine impregnation of silica 2. The effect of method of preparation, loading, and calcination temperature on (reduced) particle size. J. Catal. 2004, 225 203-212. DOI: 10.1016/j.jcat.2004.04.007.
12. Vít, Z.; Gulková, D.; Kaluža, L.; Boaro, M. Effect of catalyst precursor and its pretreatment on the amount of β-Pd hydride phase and HDS activity of Pd-Pt/silica-alumina. Appl. Catal. B. Environ. 2014, 146, 213-220. DOI: 10.1016/j.apcatb.2013.02.055.
13. Hernández Morales, R.; Pacheco Sosa, J.G.; Torres Torres, J.G.; Pérez Vidal, H.; Lunagómez Rocha, M.A.; De la Cruz Romero, D. Pt/Ga-SBA-15 composites synthesis and characterization. Superf. y Vacío 2020, 33, 1-8. DOI: 10.47566/2020_syv33_1-200301.
14. Ellerbrock, R.; Stein, M; Schaller, J. Comparing amorphous silica, short-range-ordered silicates and silicic acid species by FTIR. Sci . Rep. 2022, 12, 11708. DOI: 10.1038/s41598-022-15882-4.
15. Han, Y.; Wen, B.; Zhu, M.; Dai. B. Lanthanum incorporated in MCM-41 and its application as a support for a stable Ni-based methanation catalyst. J. Rare Earths 2018, 36(4), 367-373. DOI: 10.1016/j.jre.2017.07.016.
16. Giraldo, L.; Bastidas-Barranco, M.; Moreno-Piraján, J.C. Vapour Phase Hydrogenation of Phenol over Rhodium on SBA-15 and SBA-16. Molecules 2014, 19, 20594-20612. DOI: 10.3390/molecules191220594.
17. Gregg, S.J.; Ramsay, J.D.F.; A Study of the Adsorption of Carbon Dioxide by Alumina Using Infrared and Isotherm Measurements. J. Phys. Chem. 1969, 73, 1243-1247. DOI:10.1021/J100725A011.
18. Parkyns, N.D. The Influence of Thermal Pretreatment on the Spectrum of Carbon Dioxide Adsorbed on Alumina. J. Phys. Chem. 1971, 76, 526-531. DOI: /10.1021/j100674a014.
19. Escobar, J.; Ramírez, J.; Cuevas, R.; Ángeles, C.; Barrera, M.C.; Gutiérrez, A. Thiophene HDS on La-Modified CoMo/Al_2O_3 Sulfided Catalysts. Effect of Rare-Earth Content. Top. Catal. 2020, 63, 529-545. DOI:10.1007/s11244-020-01326-8.
20. Hungría, A.B.; Calvino, J.J.; Hernández-Garrido, J.C. HAADF STEM Electron Tomography in Catalysis Research. Top. Catal. 2019, 62, 808-821. DOI: 10.1007/s11244-019-01200-2.
21. Ballesteros-Plata, D.; Infantes-Molina, A.; Rodríguez-Castellón, E. Study of bifunctionality of Pt/SBA-15 catalysts for HDO of Dibenzofuran reaction: Addition of Mo or use of an acidic support. Appl. Catal. A-Gen 2019, 580, 93-101. DOI: 10.1016/j.apcata.2019.05.002.
22. Wang, C.-Y.; Ra, J.; Shen, K.; Vohs, J.M.; Gorte, R.J. Hydrodeoxygenation of m-Cresol over WO_x-Pt/SBA-15 Using Alkanes as Hydrogen Carriers. ACS Catal. 2023, 13(16), 10908-10915. DOI: 10.1021/acscatal.3c01636.
23. Ballesteros-Plata, D.; Barroso-Martín, I.; Medina Cervantes, J.A.; Maciel, C.; Huirache-Acuña, R.; Rodríguez-Castellón, E.; Infantes-Molina, A. Bimetallic Niobium-Based Catalysts Supported on SBA-15 for Hydrodeoxygenation of Anisole. Ind. Eng. Chem. Res. 2021, 60(51), 18831-18840. DOI: 10.1021/acs.iecr.1c02799.
24. Feliczak-Guzik, A.; Szczyglewska, P.; Nowak, I. The effect of metal (Nb, Ru, Pd, Pt) supported on SBA-16 on the phenol Hydrodeoxygenation. Catal. Today 2019, 325, 61-67. DOI: 10.1016/j.cattod.2018.06.046.

25. Shivhare, A.; Hunns, J.A.; Durndell, L.J.; Parlett, C.M.A.; Isaacs, M.A.; Lee, A.F.; Wilson, K. Metal-Acid Synergy: Hydrodeoxygenation of Anisole over Pt/Al-SBA-15. ChemSusChem 2020, 13, 4945-4953. DOI: 10.1002/cssc.202000764.
26. Novodarszki, G.; Lónyi, F.; Csík, B.; Mihályi, M.R.; Barthos, R.; Valyon, J.; Vikár A.; Deka, D.; Pászti, Z.; Shi, Y.; Solt, H.E. Hydroconversion of lignin-derived platform compound guaiacol to fuel additives and value-added chemicals over alumina-supported Ni catalysts. Appl. Catal. A-Gen 2024, 680, 119757. DOI: 10.1016/j.apcata.2024.119757.
27. Infantes-Molina, A.; Pawelec, B.; Fierro, J.L.G.; Loricera, C.V.; Jiménez-López, A.; Rodríguez-Castellón. Effect of Ir and Pt Addition on the HDO Performance of RuS_2/SBA-15 Sulfide Catalysts. Top. Catal. 2015, 58, 247-257. DOI: 10.1007/s11244-015-0366-0.
28. Jeon, M.-J.; Jeon, J.-K.; Suh, D.J.; Park, S.H.; Sa, Y.J.; Joo, S.H.; Park, Y.-K. Catalytic pyrolysis of biomass components over mesoporous catalysts using Py-GC/MS. Catal. Today 2013, 204, 170-178. DOI: 10.1016/j.cattod.2012.07.039.
29. Escobar, J.; Barrera, M.C.; Valente, J.S.; Solís-Casados, D.A.; Santes, V.; Terrazas, J.E.; Fouconnier, B.A.R. Dibenzothiophene Hydrodesulfurization over P-CoMo on Sol-Gel Alumina Modified by La Addition. Effect of Rare-Earth Content. Catalysts 2019, 9(4), 359. DOI:10.3390/catal9040359.
30. Cui, J.-W.; Massoth, F.E.; Topsøe, N.Y. Studies of Molybdena-Alumina Catalysts XVIII. Lanthanum-Modified Supports. J. Catal. 1992, 136, 361-377. DOI: 10.1016/0021-9517(92)90068-S.
31. Terrab, I.; Ouargli, R.; Boukoussa, B.; Ghomari, K., Hamacha, R.: Roy, R.; Azzouz, A.; Bengueddach, A. Assessment of the intrinsic interactions of mesoporous silica with carbon dioxide. Res Chem. Intermed. 2017, 43, 3775-3786. DOI: 10.1007/s11164-016-2846-7.
32. Boukoussa, B.; Hakiki, A.; Nunes-Beltrao, A. P.; Hamacha, R.; Azzouz, A.Assessment of the intrinsic interactions of nanocomposite polyaniline/SBA-15 with carbon dioxide: Correlation between the hydrophilic character and surface basicity. J. CO2 UTIL. 2018, 26, 171-178. DOI: 10.1016/j.jcou.2018.05.006.
33. Bartz, W.; Górka, M.; Rybak J.; Rutkowski, R.; Stojanowska, A. The assessment of effectiveness of SEM-EDX and ICP-MS methods in the process of determining the mineralogical and geochemical composition of particulate matter deposited on spider webs. Chemosphere 2021, 278, 130454. DOI: 10.1016/j.chemosphere.2021.130454.